

An experimental streamflow reconstruction for the River Murray, Australia, 1783–1988

Ailie J. E. Gallant¹ and Joëlle Gergis¹

Received 30 July 2010; revised 21 January 2011; accepted 17 February 2011; published 26 April 2011.

[1] We present an experimental reconstruction of River Murray streamflow to assess present-day variations in the context of the past two centuries. Nine annually resolved paleoclimate proxy records from the Australasian region are used to develop a reconstruction of streamflow from 1783 to 1988. An ensemble of reconstructions is presented, providing probabilistic estimates of River Murray flows for each year back in time. The best-estimate reconstruction captures approximately 23% (50%) of annual (decadal) naturalized streamflow variability. High and low streamflow phases and their association with decadal climate variability in the Pacific are discussed. Reconstructed River Murray streamflow shows considerable variation since 1783. We estimate that there is a 2.3% chance that the 1998–2008 record low decadal streamflow deficit has been exceeded since European settlement. Stochastic simulations of the decadal variations in River Murray streamflow are computed using the paleostreamflow reconstruction to estimate model parameters. From these simulations, we estimate that the 1998–2008 streamflow deficit has an approximate 1 in 1500 year return period. As climate models are assessed relative to short instrumental records, future projections of decadal-scale variations in Murray-Darling Basin (MDB) streamflow may be inadequately represented. Given the immense socioeconomic importance of Australia’s “food bowl,” future paleoclimate and modeling efforts should be directed at understanding variability at this scale. This would greatly enhance our capacity to estimate regional sensitivity of the MDB’s hydroclimate to further anthropogenic influences.

Citation: Gallant, A. J. E., and J. Gergis (2011), An experimental streamflow reconstruction for the River Murray, Australia, 1783–1988, *Water Resour. Res.*, 47, W00G04, doi:10.1029/2010WR009832.

1. Introduction

[2] The Murray-Darling River system and its tributaries form a vast catchment covering around 1×10^6 km² in southeast Australia (Australian Bureau of Statistics, Water and the Murray-Darling Basin—A statistical profile, 2000–01 to 2005–06, 2010, <http://www.abs.gov.au/AUSSTATS/abs@.nsf/mf/4610.0.55.007>, hereafter referred to as ABS, online report, 2010). The River Murray, which forms the southern portion of the basin, runs for almost 2500 km across the heavily populated states of New South Wales, Victoria, and South Australia. As such, it is a complex economic and natural resource of immense importance to the livelihood of a diverse group of stakeholders.

[3] The River Murray’s highly variable streamflow in part reflects the region’s erratic natural rainfall variability and flow regulation engineered to support urban water supplies, agriculture, and hydroelectricity generation [Murphy and Timbal, 2008]. Although the Murray-Darling Basin (MDB) receives an average annual rainfall equivalent of 530,618 GL, 94% of this total evaporates or transpires, a further 2%

provides groundwater recharge, and the remaining 4% becomes runoff feeding streamflow (ABS, online report, 2010). Intensive irrigation systems draw water from the River Murray to support approximately 40% of Australia’s total agricultural production and nearly 70% of all irrigated crops and pastures [Hennessy *et al.*, 2007].

[4] The streamflow losses in the river system are being exacerbated by a prolonged drought in the region, which was in its 13th year during 2010. Determining the extent to which the prolonged drought in the region is caused by natural decadal-scale variability and/or anthropogenic climate change is now a major research priority. According to the Intergovernmental Panel on Climate Change’s Fourth Assessment Report, annual streamflow in the MDB is likely to fall 10%–25% by 2050 and 16%–48% by 2100 [Hennessy *et al.*, 2007]. At present, the decadal scale streamflow deficit is approximately 50% below the 1892–2008 average on the basis of streamflow data from the Murray-Darling Basin Authority (MDBA) detailed in section 2.1.2. This figure already exceeds the “worst-case scenario” estimates of the 2100 climate change projections for the region. The short length of instrumental records (around 100 years) limits our comparisons of decadal-scale natural variability with climate models, making our understanding of its causes and distinguishing it from anthropogenic climate change difficult. Consequently, there is need to investigate the nature

¹School of Earth Sciences, University of Melbourne, Melbourne, Australia.

Table 1. Proxy Data From the Australasian Region Used in This Study, A.D. 1783–1988^a

Proxy Data	Dates	Location	Proxy Variable	Reference(s)
Kauri tree rings	1724 B.C. to A.D. 2002	New Zealand	total ring width	<i>Fowler et al.</i> [2008]
Teak tree rings	1565–2000	Indonesia	total ring width	<i>D'Arrigo et al.</i> [2006]
Western Australia <i>Callitris</i> tree rings	1655–2005	SW Australia	total ring width	<i>Cullen and Grierson</i> [2009]
Huon pine tree rings	1600 B.C. to A.D. 1991	SE Australia	total ring width	<i>Cook et al.</i> [2000]
Celery top pine tree rings, western Tasmania	1290–1998	SE Australia	total ring width	<i>Allen et al.</i> [2001], <i>Allen</i> [2002], <i>La Marche et al.</i> [1979]
Celery top pine tree rings, eastern Tasmania	1152–1994	SE Australia	total ring width	<i>Allen et al.</i> [2001], <i>Allen</i> [2002], <i>La Marche et al.</i> [1979]
Fiji-Tonga corals	1650–2001	SW Pacific	δO^{18} (four core average)	<i>Linsley et al.</i> [2008]
Great Barrier Reef corals	1631–1983	NE Australia	luminescence (Oct–Sep)	<i>Lough</i> [2007]
Bali corals	1782–1989	SW Pacific	δO^{18}	<i>Charles et al.</i> [2003]

^aAll records are dated to the calendar year with the exception of the Great Barrier Reef “master” coral chronology, which is dated to an October–September year, and the Bali corals, which are dated to a June–August year.

and causes of hydroclimatic variability in the MDB on low-frequency (decadal or longer) time scales.

[5] In Australia, digitized climate observations extend back to the late 19th century at best, which provides us with a relatively brief snapshot of long-term hydroclimatic variability. Climatically sensitive, annually resolved climate proxies like tree rings, coral, ice cores, and speleothems (cave records) can assist in defining the bounds of climate variability needed for the efficient long-term management of natural resources. Most importantly, paleoclimate records allow us to improve the estimation of natural climate variability now being forced by additional anthropogenic factors.

[6] In particular, paleoclimate research of the most recent 2000 or so years allows the range of natural climate variability to be estimated under preindustrial boundary conditions. Currently, the spatiotemporal nature and magnitude of such variability in the Australian region is poorly understood because of the lack of regional syntheses of paleoclimate data. Well-dated, high-resolution paleodata can offer a critical test of global circulation models by providing extended estimates of annual–decadal climate variability not captured by instrumental observations. In this way, past analogues found in paleoclimate reconstructions can be used to constrain climate model projections [*Hegerl et al.*, 2006, 2007; *Seager*, 2007], aiding in the reduction of the uncertainty of regional climate change projections. This may be particularly important for the MDB, where recent studies of instrumental records and model output have shown that water availability in the MDB may be vulnerable to further anthropogenically forced climate change, but is still an area of active research [*Hennessy et al.*, 2008].

[7] Only two previous decadal reconstructions of the MDB hydroclimate exist, primarily because of the lack of records in the region itself. *McGowan et al.* [2009] reconstructed inflow to the headwaters of the River Murray using a single reconstruction of the Pacific Decadal Oscillation (PDO), a measure of decadal-scale climate variability in the Pacific based on Chinese documentary records [*Shen et al.*, 2006]. Similarly, using a paleoreconstruction of interannual and interdecadal variability in the Pacific, *Verdon and Franks* [2007] inferred long-term hydroclimatic variability in the Lachlan River Valley in the central MDB. However, these studies assumed that MDB hydroclimate predictability is dependent on the phase of decadal-scale oscillations in the Pacific only [*Power et al.*, 1999; *Kiem and Franks*, 2004], and influences from other sources of hydroclimatic variability on the River Murray were not quantified.

[8] To assist the water industry’s need for extended estimates of the MDB’s past hydroclimatic variability, we introduce an experimental multiproxy reconstruction of River Murray streamflow back to 1783. We begin by assessing the ability of nine annually resolved paleoclimate records to reproduce annual and decadal variability of naturalized streamflow over the 1892–1988 period. We discuss a series of important caveats on the reconstruction technique and implications for the interpretation of our results. We then provide an experimental reconstruction of Murray River streamflow back to 1783, identifying key high- and low-streamflow phases and links with decadal climate variability in the Pacific. We conclude by presenting an historical perspective on extreme high and low streamflow levels recorded in the instrumental period.

2. Reconstructing River Murray Streamflow

2.1. Data Sources

2.1.1. Paleoclimate Data

[9] The lack of annually resolved paleoclimate records currently available directly from the MDB region means that records must be selected from a wider Australasian region (Table 1). All records show published sensitivities to either regional- or large-scale circulation features important to the MDB, such as the El Niño–Southern Oscillation (ENSO). However, it is important to recognize that using large-scale regional climate records to infer changes to localized streamflow ignore important land surface conditions (soil moisture, vegetation cover, and groundwater recharge) [*Chiew et al.*, 1998; *Kiem and Verdon-Kidd*, 2010]. Therefore, this experimental reconstruction is able to provide streamflow estimates only from climate-related components (e.g., rainfall, temperature, and circulation changes) of the more complex coupled hydroclimate system.

[10] All tree ring records are regional “master chronologies” calculated as the means of multiple detrended core samples from many trees for a number of sites. Note that *Phyllocladus aspleniifolius* (celery top pine) data were processed separately as eastern and western composites to reflect the strong rainfall gradient present across Tasmania [*Allen*, 2002]. To remove biological growth trends, raw total ring width measurements were detrended using 20 year cubic splines (50% variance cutoff at 20 years). This specifically targets interannual to decadal streamflow variations, thus excluding frequencies greater than 20 years.

Table 2. Instrumental Data From the Closest Possible Locations to the Proxies Listed in Table 1^a

Proxy Data	Pseudoproxy Station	Location	Optimal Variable ^b
Kauri tree rings	Auckland Aero, New Zealand	37.00°S, 174.80°E	<i>P</i>
Teak tree rings	Iswahyudi Madiun, Indonesia	7.62°S, 111.52°E	SLP
Western Australia <i>Callitris</i> tree rings	Kalgoorlie AMO, Australia	30.78°S, 121.47°E	SLP
Huon pine tree rings	Maatsuyker Island Lighthouse, Australia	43.65°S, 146.27°E	<i>T</i>
Celery top pine tree rings, western Tasmania	Hobart Airport WSO, Australia	42.83°S, 147.50°E	<i>P</i>
Celery top pine tree rings, eastern Tasmania	Launceston Airport WSO, Australia	41.55°S, 147.20°E	<i>P</i>
Fiji-Tonga corals	Nandi Aero, Fiji	17.80°S, 177.50°E	SST
Great Barrier Reef corals	Mackay MO, Australia	21.12°S, 149.22°E	SLP
Bali corals	Tuban/Denpasar, Indonesia	8.80°S, 115.20°E	SLP

^aThe station name and location, the corresponding paleoproxy station, and the optimal variable selected for use in the pseudoproxy analysis (section 2.2.1) are listed.

^b*P*, precipitation; SLP, sea level pressure; *T*, temperature; SST, sea surface temperature.

[11] With the exception of two coral records, annual means of the monthly coral data were generated for each calendar year to match the tree ring dating. However, a Great Barrier Reef composite coral luminescence reconstruction [Lough, 2007] was provided as an October–September monsoon-sensitive year. The Bali core record [Charles *et al.*, 2003] represents the June–August $\delta^{18}\text{O}$ average to capture notably higher correlations with observed climate indices (not shown). As Lough’s [2007] Great Barrier Reef coral record was not available in “raw,” format, it was assessed using only the “climate window” identified in their original publications.

[12] The sensitivity of the proxy records to climate may not be specific to a time period that spans the traditional calendar year, leading to slight dating discrepancies between records. As such, lag correlations were computed against the leading principal component (described in section 2.2) and each proxy to establish synchronicity with the climate signal. As a result, the Huon pine tree ring chronology was advanced by 1 year.

2.1.2. Instrumental Data: Streamflow and the Interdecadal Pacific Oscillation

[13] Monthly streamflows for the River Murray were provided by the Murray-Darling Basin Authority for the 1892–2009 period. Murray system inflows (excluding Menindee inflows and Snowy releases) represent the sum of the water entering the River Murray upstream of the Darling and excluding regulated releases from the Snowy hydroelectric scheme (most of which are derived from another catchment). Systems used in the streamflow calculation include the Dartmouth Reservoir, Hume unregulated inflows (excluding the Snowy scheme and Dartmouth releases), Kiewa at Bandiana, Ovens at Peechelba, Broken Creek at Rices Weir, Goulburn River at McCoy’s Bridge, Campaspe at Rochester, Billabong Creek at Darlot, Loddon River at Appin South, and the Murrumbidgee River at Balranald (Anthony Scott, MDBA, personal communication, 2010).

[14] The historical streamflow data (hereafter referred to as “naturalized streamflow”) includes a mixture of instrumental streamflow measurements (2000–2009) and modeled streamflow (1892–1999). The modeled data represent approximations of unaltered streamflow in tributaries and catchments that have been affected by human activity, including extractions and landscape changes; e.g., agricultural practices and land clearing were extensive through the Goulburn and Murrumbidgee catchments (Anthony Scott, MDBA, personal communication, 2010). Although data are

updated in line with changing operations and model revisions, considerable uncertainty still exists from contributions from farm dams and catchments changes. However, we were unable to quantify these contributions. Despite this uncertainty, the River Murray streamflow data used here have been used elsewhere [Power *et al.*, 1999; Cai and Cowan, 2008; McGowan *et al.*, 2009] and represent the best estimates currently available.

[15] To investigate the influence of decadal-scale climate oscillations on River Murray streamflow, we analyze its relationships with the Interdecadal Pacific Oscillation (IPO), a Pacific-wide ocean-atmosphere oscillation on the 15–30 year time scale [Power *et al.*, 1999]. Here, decadal-scale Pacific variability is represented by the unfiltered monthly IPO anomaly normalized to a 1911–1995 base period (http://www.iges.org/c20c/IPO_v2.doc) averaged over a August–July year and smoothed using an 11 year running mean.

2.1.3. Instrumental Data: Pseudoproxies

[16] Mean temperature, precipitation, sea level pressure (SLP), and sea surface temperatures (SSTs) were used as possible variables that are sensitive to the same large-scale forcing as River Murray streamflow variability. Monthly mean temperature and precipitation data were obtained from the Global Historical Climate Network (GHCN) of stations [Peterson and Vose, 1997]. The stations chosen were those closest to the locations of the climate proxy data (Table 2). Because of the short length of record of sea level pressure data at the candidate GHCN stations, the National Centers for Environmental Prediction reanalysis SLP data from the grid point closest to the paleoproxy record were used [Kalnay *et al.*, 1996]. SST data were obtained from the nearest grid cell in the HadISST data set [Rayner *et al.*, 2003]. The GHCN station data spanned different time periods and contained missing data, so to optimize data availability, the pseudoproxy stations were examined only over the period 1948–1993.

2.2. Reconstruction Method

[17] A River Murray streamflow reconstruction was developed by assuming that the large-scale mechanisms regulating climate variations in several key, remote locations are also responsible for driving a significant proportion of the annual- and decadal-scale variations in River Murray streamflow [Chiew *et al.*, 1998; Power *et al.*, 1999; Kiem *et al.*, 2003; Kiem and Franks, 2004; Verdon and Franks, 2007; McGowan *et al.*, 2009]. The climate of the River Murray

region responds primarily to atmosphere–ocean interactions stemming from the Pacific, Indian, and Southern Oceans [Risbey *et al.*, 2009]. We propose that (1) a common climate signal from these sources will reproduce a significant proportion of the variability in River Murray streamflow and (2) the climate proxies in Table 1 represent local climate variations that are sensitive to this common, large-scale forcing and can therefore be used to reconstruct River Murray streamflow. To test the viability of using a remote climate network to reconstruct streamflow, we examine the suite of instrumental climate data at the same locations as the proxy data that were described in section 2.1.3, hereafter referred to as “pseudoproxies.” The methodology used to reconstruct streamflow using climate and pseudoproxies is briefly described here, with further detail provided in sections 2.2.1 and 2.2.2.

[18] The large-scale climate fluctuations that are common to interannual and interdecadal variations in both River Murray streamflow and the remote station network were extracted using principal component analysis (PCA) [Jolliffe, 2002]. PCA was applied to the nine paleoclimate and corresponding pseudoproxy records listed in Tables 1 and 2. In any PCA, the lower-order principal components (PCs) contain the most coherence (in this case, the common large-scale physical climatic signal), while the higher-order PCs generally contain noise. Therefore, only the lower-order PCs should be retained for analysis. However, deciding on how many PCs to retain is difficult. Too few PCs, and important aspects of the real signal may be excluded, but including too many can introduce extraneous noise.

[19] North *et al.* [1982] proposed a method to retain PCs with coherent and physically realistic signals only, which is now commonly used in PCA. This involved comparing the variance explained by successive PCs (the eigenvalues). If the eigenvalues are statistically similar, then the latter PC displays an ambiguous signal (see North *et al.* [1982] for further details). However, North *et al.*'s [1982] method compared the spread of eigenvalues for each PC derived from idealized Gaussian simulations. In the case of the climate proxies analyzed here, all data were normally distributed. However, several records had significant autocorrelations at a lag of 1 year (not shown) and hence were not considered independent, making North *et al.*'s [1982] method unsuitable for our data.

[20] Instead, we used a modification of the above method. Originally proposed by Kestin [2001], the method preserves the realistic statistical characteristics of the data distribution by using the data itself to identify ambiguous PCs. In this case, instead of using idealized simulations to estimate statistically significant differences between eigenvalues for each PC, we subsampled the paleodata by randomly removing 10% of the data as a block to retain a realistic autocorrelation. This was done 1000 times, the eigenvalues were recomputed, and a 95% confidence interval was generated. If the confidence intervals between two successive PCs overlapped, the latter PC was considered degenerate. The threshold for PC retention was determined from the presence of the first degenerate eigenvalue. Subsequently, this degenerate PC, and all remaining higher-order PCs, were ignored.

[21] The retained PCs were assumed to represent the large-scale climate signals associated with River Murray streamflow variability. These lower-order PCs were then

projected onto instrumental River Murray streamflow using multiple linear regression, expressed as

$$S_t = \sum_{n=1}^{n=N} \alpha_n \phi_{n,t} + \varepsilon_t, \quad (1)$$

where reconstructed streamflow (S_t) at time t is the sum of the combined n th regression coefficients ($\alpha_{n,t}$) for the n th higher-order principal components ($\phi_{n,t}$) and the residual error term (ε_t).

[22] All PCs extracted from the paleoproxy and pseudoproxy data were normally distributed. However, the distribution of naturalized streamflow data was distinctly non-normal, displaying a leptokurtic (higher than normal peak, $\gamma_2 = 5.97$) distribution, with a heavy positive skew (to the right, $\gamma_1 = 2.07$). The implications of this meant that regression of the PCs against the raw data would produce a spurious reconstruction. Consequently, a natural log transform was applied to the naturalized streamflow data prior to their regression against the PCs. The resulting transformed naturalized streamflow distribution was close to normal, with skewness (γ_1) reduced to 0.11 and kurtosis (γ_2) reduced to 3.32 (a normal distribution has $\gamma_1 = 0.0$ and $\gamma_2 = 3.0$). The regression coefficients for the streamflow reconstruction (equation (1)) were then calculated by regressing the raw PCs against the transformed naturalized streamflow data.

[23] In the case of the climate proxies, when applying the regression algorithm, the coefficients were derived using a subsample of the PC time series as the calibration series. The remaining data were then used to validate the resulting reconstruction as they were independent of the training period. As a conservative approach we selected 50 years, or approximately half the data, for calibration and used the remaining 47 years for verification. The 50 year calibration period was selected as 5 decades to preserve both decadal-scale variations and interannual persistence ($r = 0.37$ at a lag of 1 year from 1892 to 1988) in the naturalized streamflow. The choice of calibration period was arbitrary but, as discussed in section 2.2.2, this choice has a significant impact on the apparent skill of the reconstruction. To avoid the issue of overfitting the regression model to a single calibration period, we use bootstrap resampling to develop an ensemble of paleostreamflow reconstructions, each time selecting 5 random decades from which to derive the regression coefficients. A decade was defined as beginning in any year between 1892 and 1988, which was the period common to both the naturalized streamflow and paleoproxy data. This identified 87 possible decades, five of which were randomly selected at any one time for calibration.

[24] Following the regression, both the naturalized streamflow and resulting reconstruction (S in equation (1)) were inverted (i.e., the exponent was taken) so that the streamflow reconstruction was reconverted into its original form. Prior to the generation of the reconstruction, all data were normalized relative to the 1948–1993 period of common overlap for the pseudoproxy data (section 2.2.1) and 1892–1988 for the climate proxy data (section 2.2.2). Finally, the reconstruction was rescaled to have the same mean and variance as naturalized streamflow in giga-liters.

[25] For the paleoclimate proxies a 10,000-member reconstruction ensemble was generated, with each member contributing an estimate of the sensitivity of the errors in the

Table 3. Eigenvector Loadings for Individual Proxies Constituting PCs 1 and 2 of the Paleoclimate Network and the Loadings for PCs 1, 2, and 3 From the Instrumental Network Used for Pseudoproxy Analysis^a

Proxy locations	Paleoclimate Network		Instrumental Network		
	PC1 _{paleo}	PC2 _{paleo}	PC1 _{instrum}	PC2 _{instrum}	PC3 _{instrum}
Kauri tree rings	0.21	-0.17	-0.12	0.18	0.17
Teak tree rings	0.23	-0.40	0.26	-0.16	0.01
Western Australia <i>Callitris</i> tree rings	-0.29	0.04	-0.24	0.14	0.44
Huon pine tree rings	0.24	-0.17	-0.95	-0.42	-0.14
Celery top pine tree rings, western Tasmania	-0.46	0.15	-0.44	0.44	-0.56
Celery top pine tree rings, eastern Tasmania	0.54	0.75	0.15	-0.05	-0.02
Fiji-Tonga corals	0.11	-0.52	0.15	-0.76	0.54
Great Barrier Reef corals	0.62	0.13	-0.33	-0.09	1.73
Bali corals	0.02	0.10	0.37	4.49	0.33
Total variance explained	22%	16%	53%	12%	10%

^aThe loadings describe the relative importance of each of the locations to the principal component.

reconstruction from two sources. The first source is errors associated with the arbitrary selection of the calibration period used to determine the regression coefficients (α_n), hereafter termed the “calibration error.” Resampling of the 5 decades used for calibration was performed with replacement. However, the resulting spread of decades chosen formed a uniform distribution. Therefore, the uncertainty in the ensemble has not been underestimated because of biases in the choice of decades selected for calibration. The second source of error in the reconstruction relates to the residual errors (ε in equation (1)) between the reconstructed and naturalized streamflow data, representing aspects of streamflow that could not be captured by the large-scale climate signal (e.g., local weather noise, land surface properties, and local surface hydrology), hereafter termed the “residual error.”

[26] A suite of metrics was then used to estimate the skill for each of the 10,000 River Murray streamflow reconstructions [Cook and Kairiukstis, 1990]. Skill was assessed using the data with which the model was calibrated and data from the independent verification period. The metrics used were the Pearson correlation coefficient (r), variance explained adjusted for degrees of freedom (ar^2), root-mean-square error (RMSE), the reduction of error (RE), the coefficient of efficiency (CE), and the sign test (ST). Refer to Cook and Kairiukstis [1990] and Fritts [1976] for a comprehensive description of these statistical measures.

2.2.1. Reconstructing River Murray Streamflow Using Remote Instrumental Observations: A Pseudoproxy Experiment

[27] Prior to reconstructing River Murray streamflow using paleoclimate proxies, we assessed the viability of using a remote climate network to develop a streamflow reconstruction. The pseudoproxy analysis tests (1) which local climate variables are associated with the common large-scale climate variations in the paleoclimate proxy network and (2) whether these local climate variations can be used to reconstruct River Murray streamflow from instrumental data.

[28] First, we examined the relationships between the common signal contained in the paleoclimate proxies and the instrumental climate data at stations close to the locations of the paleoclimate records (Table 2). Mean temperature, precipitation, SLP, and SSTs (at locations of coral data only) were chosen as candidate variables. The climate variables at each remote location were correlated against the leading PC from the paleoclimate proxy network to determine which variable is most closely associated with the common signal

extracted from the paleoclimate network, as shown in Table 2. The optimal climate variables at each location were then used to reconstruct River Murray streamflow as outlined in section 2.2.2.

[29] Using the adapted methodology by Kestin [2001] for selecting PCs with a realistic climate signal (described in section 2.2), the first three principal components were chosen. The eigenvector loadings of each of the PCs for each location are shown in Table 3. Multiple regression was applied using the full record (1948–1993) for calibration. Figure 1 shows the resulting annual and decadal reconstructions of River Murray streamflow from 1948 to 1993 that were developed from the optimal network of instrumental data at nearby stations to the paleoclimate data.

[30] The skill metrics of the pseudoproxy reconstruction are shown in Table 4. There is significant skill in both annual and decadal streamflow reconstructions. Note that the verification correlation ($r_{\text{verification}}$) and the CE statistic could not be computed as both require independent data. Figure 1

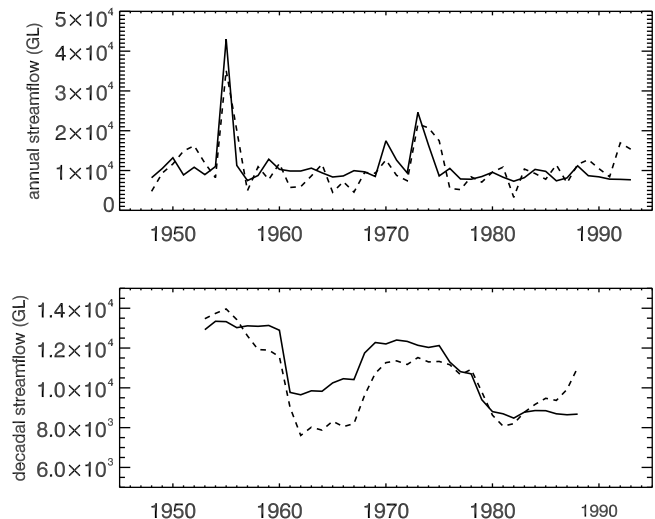


Figure 1. An annual and decadal streamflow reconstruction for the River Murray, generated from climate data at nine remote stations that correspond to the locations of the paleoproxy data (Table 2). The solid line represents the streamflow reconstructed from the paleoclimate proxies, and the dashed line represents streamflow from the instrumental climate observations.

Table 4. Skill Metrics of the Annual and Decadal Pseudoproxy and Paleoproxy Reconstructions of River Murray Streamflow^a

Statistic	Pseudoproxies		Paleoproxies	
	Skill of the Annual Reconstruction (1892–1988)	Skill of the Decadal Reconstruction (1892–1988)	Skill of the Annual Reconstruction (1892–1988)	Skill of the Decadal Reconstruction (1892–1988)
$r_{\text{calibration}}$	0.74	0.81	0.49 (0.27, 0.63)	0.72 (0.37, 0.83)
$ar^2_{\text{calibration}}$	0.44	0.54	0.24 (0.07, 0.40)	0.48 (0.08, 0.66)
$r_{\text{verification}}$	–	–	0.46 (0.24, 0.60)	0.70 (0.30, 0.83)
RE	0.49	0.62	–0.08 (–1.03, 0.33)	0.48 (–0.43, 0.73)
CE	–	–	–0.13 (–1.64, 0.25)	0.33 (–0.72, 0.64)
ST	92%	92%	68% (55%, 79%)	75% (55%, 98%)
RMSE	0.71	0.61	1.04 (0.85, 1.24)	0.77 (0.63, 1.06)

^aThe following statistics were calculated: r is the Pearson correlation coefficient; ar^2 is square of the multiple correlation coefficient, which adjusts for the loss of degrees of freedom; RE is reduction of error statistic; CE is the coefficient of efficiency statistic; and RMSE is root-mean-square error (in standard deviations). The sign test (ST) is shown as the percentage of anomalies in agreement. Note that the CE and r (for the verification period only) could not be calculated for the pseudoproxy analysis as no data was retained for independent verification. The skill metrics for the paleoproxy analysis is given as the median of the 10,000-member reconstruction ensemble, and a 95% confidence interval is included as the error estimate in brackets.

demonstrates the ability of a remote network of climate data to be able to extract large-scale common climate signals that can be used to reconstruct a substantial portion of the variability in River Murray streamflow. Though due caution is given to the fact that the pseudoproxy network could be computed only for a 46 year period, the remote network of instrumental data captures approximately 55% of the annual variations and 66% of the decadal variations in River Murray streamflow. This confirms the feasibility of using a remote network of proxy data to reconstruct River Murray streamflow.

2.2.2. Reconstructing River Murray Streamflow Using Paleoclimate Proxy Data

[31] Following the successful reconstruction of annual and decadal River Murray streamflow from the instrumental pseudoproxy network, streamflow was reconstructed using the paleoproxies from 1783 to 1988, the period common to all records. Though each paleoproxy is annually resolved, the time period associated with each annual increment differed for each record. Thus, to determine the period with the strongest common signal, the first PC from the paleonetwork was correlated against naturalized streamflow for all possible 3, 6, 9, and 12 month averages. The strongest relationship was for the August–July year, closely matching the June–May “water year” used by water management authorities in southeast Australia. All subsequent descriptions of variations in annual streamflow refer to an August–July year.

[32] Using the adapted methodology by *Kestin* [2001] (described in section 2.2), the first two PCs of the paleoproxy network were selected for development of the streamflow reconstruction (Figure 2). Moreover, these PCs were the only two (of nine) that had statistically significant correlations (at the 95% level) with naturalized River Murray streamflow from 1892 to 1988 of -0.33 and -0.37 for PCs 1 and 2, respectively, further validating our selection.

[33] For most ensemble members, the second PC was the strongest predictor of River Murray streamflow, corresponding to its stronger relationship with naturalized streamflow. The distribution of the regression coefficients showed the median strength and spread of the contribution to the streamflow regression model is PC1, $\alpha_1 = -0.15$ and $2\sigma = 0.10$ and PC2, $\alpha_2 = -0.25$ and $2\sigma = 0.16$. The annual and decadal River Murray streamflow reconstructions are shown in Figure 3.

Calculating an 11 year running mean of each ensemble member generated the ensemble of decadal reconstructions, with error estimates calculated as 2 standard deviations of these smoothed reconstructions. The best estimate of the annual and decadal reconstructions of River Murray streamflow are represented by the median of each of the 10,000-member annual and decadal ensembles.

[34] The errors between each reconstruction ensemble member and naturalized streamflow were normally distributed. Furthermore, the distribution of the autocorrelations in the errors had a mean value of -0.005 and a standard deviation of 0.069, indicating independence. These properties indicate that the errors between the reconstruction and naturalized streamflow are likely to represent random noise rather than a process that could not be captured by the multiple-regression model.

[35] To highlight the sensitivity of the streamflow reconstruction to the chosen calibration interval, each time series was evenly split in two and model skill was determined using data from the first half (1892–1939) for calibration and latter half (1940–1988) for verification and vice versa (Table 5). Determining the regression coefficients

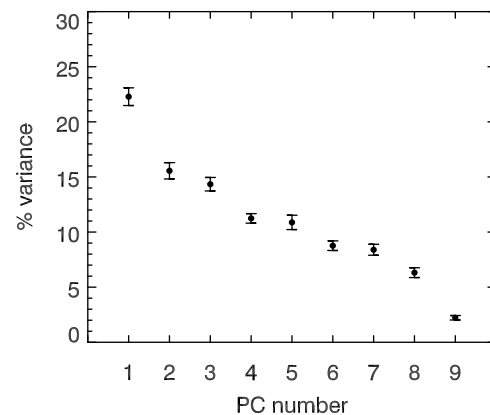


Figure 2. The percentage of the variance captured by the principal components calculated from the nine paleoclimate records listed in Table 1. Error bars represent a 95% confidence interval of the distribution of 1000 resampled eigenvalues, recomputed from the proxy data that had 10% of data randomly removed as a single block.

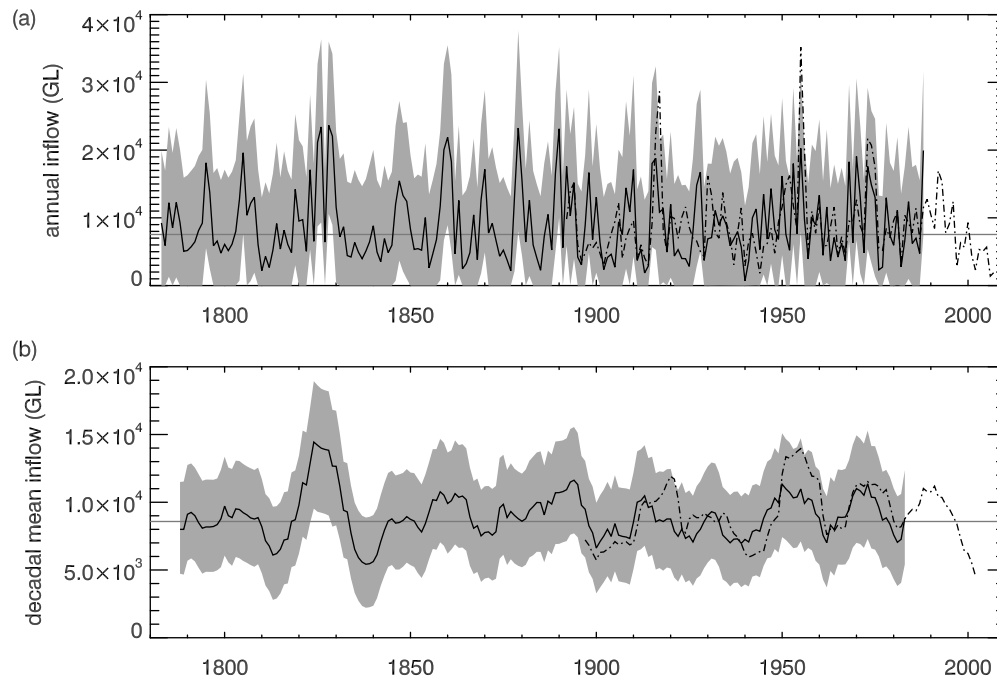


Figure 3. Paleoreconstructions of (a) annual and (b) decadal River Murray streamflow. The gray envelope represents the confidence interval for the reconstruction estimated as 2 standard deviations of the combined calibration and residual errors. The calibration errors describe errors associated with recalculating estimates of the regression parameters on the basis of the selection of the calibration period. The residual errors are calculated as the difference between the reconstruction estimate and the naturalized streamflow data. The black solid line shows the median of the ensemble reconstructions, and the dash-dotted line shows the observed River Murray streamflow from 1892 to 2008. The thin gray lines show the medians of the reconstructed annual and decadal reconstructed streamflows from 1892 to 1988, which are 7838 and 8744 GL, respectively.

using the first half of the time series as the calibration period produced strong model skill metrics in the validation period. Conversely, calibrating the model to the latter period verified poorly. Figure 4a shows that the sensitivity of the annual streamflow reconstruction to the full and split calibration periods was small compared to the residuals. However, the effects were compounded in the decadal reconstruction, and the relative size of the calibration errors compared to the residual errors increased (Figure 4b). These results indicate that the subjective selection of a single period for calibration or verification does not adequately represent the full range of model skill, strengthening the case for an ensemble approach.

[36] Given the sensitivities of the reconstruction to the calibration period, the reconstruction skill and the associated errors were calculated for each of the 10,000 ensemble members. The skill metrics described in section 2.2 are shown for the annual and decadal reconstruction ensemble in Table 4. The distribution of each metric was nonnormal, with most ensemble members displaying some (positive) skew. The best estimate of the reconstruction's skill is represented by the median of the 10,000 estimates of the metric, and a 95% confidence interval denotes the uncertainty. Figure 5 shows the frequency distributions of the calibration and residual errors associated with all ensemble members of the annual and decadal reconstructions. For the annual reconstruction, the calibration errors account for

approximately 16% of the total error. This proportion increases to 28% for the decadal reconstruction.

3. Results

3.1. Comparison of Reconstructed and Naturalized Streamflow: 1892–1988

[37] The correlation between the annual (decadal) ensemble median reconstruction and naturalized River Murray streamflow over the 1892–1988 period was 0.48 (0.71), demonstrating that the reconstruction captures approximately

Table 5. Skill Metrics as in Table 4 for the Split and Single-Period Calibration Periods

Statistics	Full-Period Calibration (1892–1988)	Early Period Calibration (1892–1940)	Late Period Calibration (1941–1988)
$r_{\text{calibration}}$	0.486	0.401	0.582
$ar^2_{\text{calibration}}$	0.220	0.124	0.310
$r_{\text{verification}}$	–	0.577	0.364
RE	–0.03	0.11	–0.120
CE	–	0.06	–0.192
ST	67%	67%	67%
RMSE	1.01	0.99	1.07

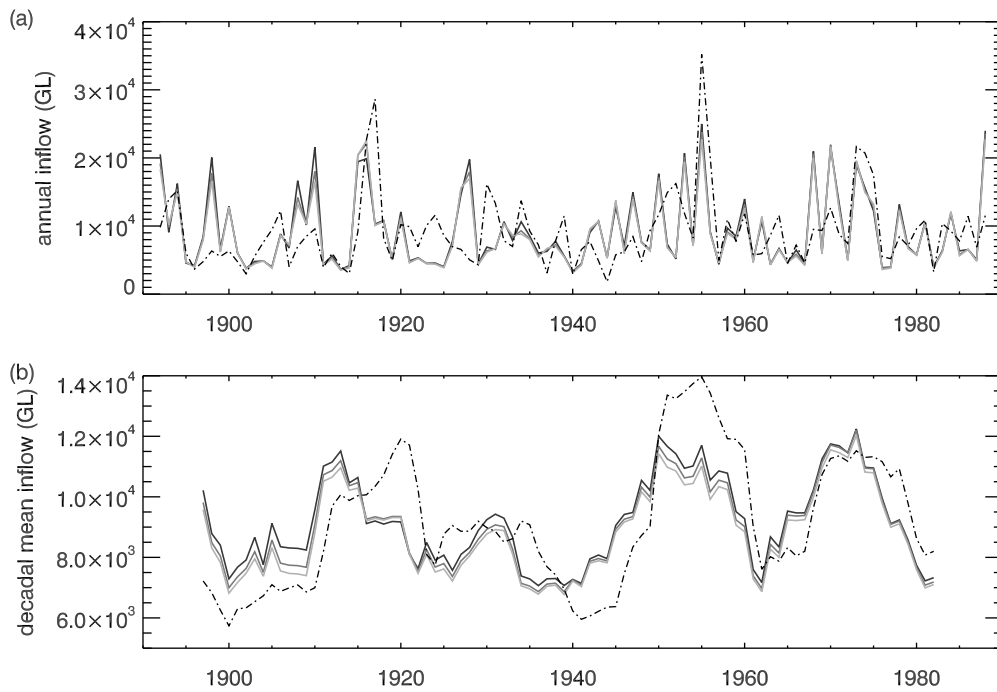


Figure 4. The (a) annual and (b) decadal reconstructions of River Murray streamflow developed using the full and split calibration. The three reconstructions highlight the importance of the choice of calibration period to the resulting reconstruction. The regression parameters for each reconstruction were calculated using data from 1941–1988 (dark gray), 1892–1940 (light gray), and 1892–1988 (medium gray). The observations are shown as the dash-dotted line.

23% (50%) of the observed annual (decadal) variations (Figure 3).

[38] The network of remote proxies was unable to capture years with very large high-flow outliers (e.g., 1916–1917, 1955, and 1973) seen in Figure 6a. These outliers reflect the inability of the reconstruction to capture the right tail skew of the observed distribution despite applying a transform, evident in Figure 6b. Conversely, the streamflow reconstruction was highly representative of the lower half of the naturalized streamflow distribution, with the transformation retaining the leptokurtic tendencies. The asymmetry in the ability of the reconstruction to capture low and high flow is seen in Figure 6, where the scatter of the data is less for the lower portions of the distribution. The ability of the remote proxy network to better capture the low-flow years may be an indication that these episodes are more closely associated with large-scale climate variations across the Australasian region, while high-flow years may be associated with more localized hydroclimate variations that are inadequately captured by remote proxies.

[39] Nevertheless, Figure 6 and Table 4 show that the remote paleoclimate network is able to capture some aspects of streamflow and can provide useful information about River Murray variability in the preinstrumental period. If we assume that the errors between the reconstruction and naturalized streamflow are representative of those throughout the reconstruction, our analysis suggests that the reconstruction is useful for assessing past changes in annual River Murray streamflow. In particular, we can be more confident that past decadal-scale River Murray streamflow variations lie within the envelope of uncertainty presented here.

3.2. Decadal Variations in Reconstructed High and Low River Murray Streamflow and Possible Links to Large-Scale Climate Forcing

[40] Having assessed the nature and limitations of the reconstruction against streamflow observations, we now turn to an assessment of decadal variations in high- and low-streamflow phases over the 1783–1988 period. As an initial comparison, all negative or positive departures at least 0.5 standard deviations from the 1892–1988 mean in the 11 year smoothed median reconstructed and naturalized

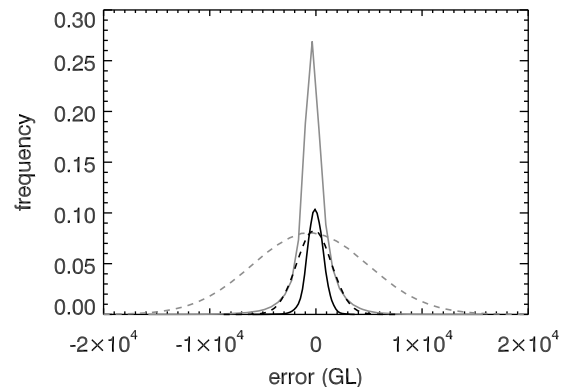


Figure 5. The distributions of annual calibration errors (solid gray line), annual residuals (dashed gray line), decadal calibration errors (solid black line), and the decadal residuals (dashed black line). All errors are described in GL.

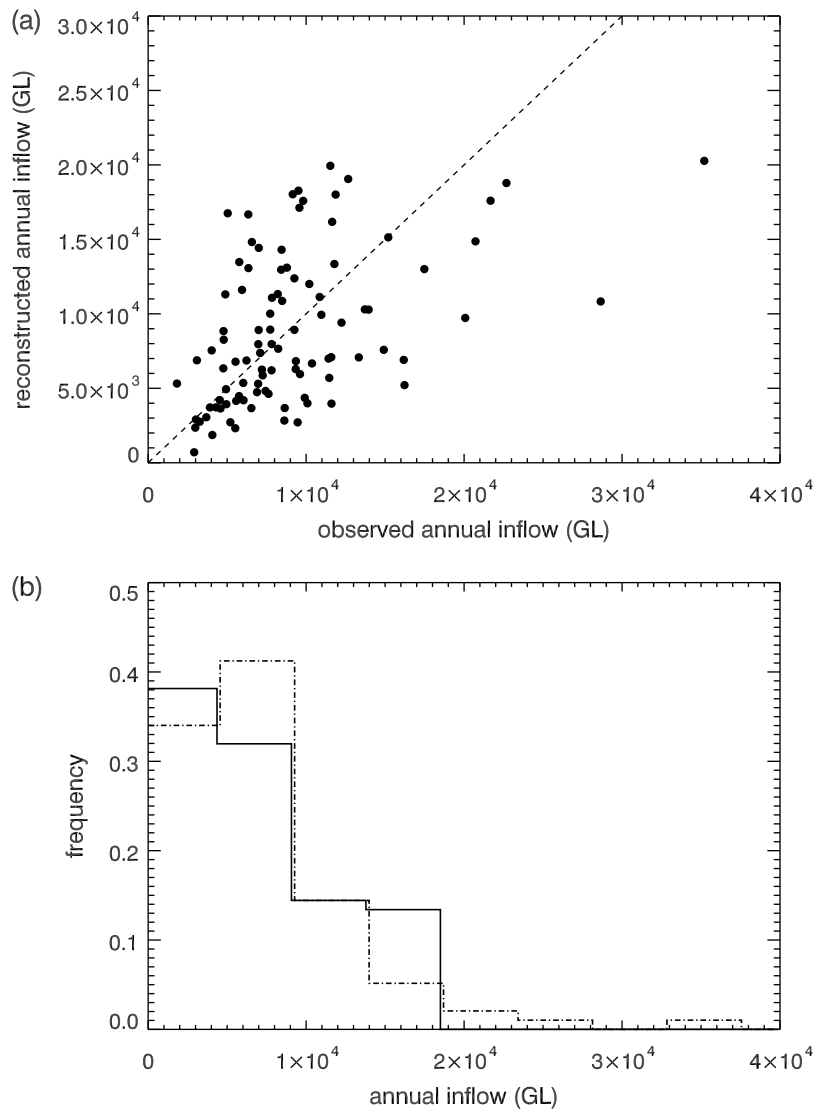


Figure 6. (a) The annual naturalized streamflow plotted against the median streamflow reconstruction, calculated as the median of the 10,000 member ensemble (in GL) and (b) the distribution of streamflow values for the observations (dash-dotted line) and the reconstruction (solid line). The observations have been slightly offset to distinguish the two histograms. Both plots were generated using data from 1892–1988.

River Murray streamflow time series were examined. The decadal naturalized streamflow observations displayed the following high- and low-streamflow sequences: 1897–1911 (low), 1917–1922 (high), 1937–1946 (low), 1950–1960 (high), 1962–1966 (low), 1969–1978 (high), 1988–1993 (high), and 1998–2003 (low). The reconstructed high- and low-streamflow periods captured most of the periods in the naturalized record, varying only slightly in terms of year of onset or total duration (Table 6).

[41] During the time of first European settlement of Australia in the late 18th century, the River Murray displayed mostly average to low streamflow conditions until the turn of the century, when near-normal conditions prevailed. Low flows occurred between 1810 and 1817 before the dry spell broke spectacularly around 1820. The reconstruction suggests that the River Murray experienced a period of very high streamflows (over 4 standard deviations above the 1892–1988 average) in the decades from 1820 to 1831 before culminating in the very dry 1834–1843 period.

[42] Aside from brief low-flow periods from 1852 to 1853 and from 1867 to 1873, the middle to late 19th century was generally characterized by normal or high streamflow conditions. The two notable protracted dry periods identified in the instrumental record, the Federation drought (~1895–1902) and World War II drought (~1937–1945) [Verdon-Kidd and Kiem, 2009], are both associated with low-streamflow periods in the reconstruction (Table 6 and Figure 3). The high-flow periods of naturalized streamflow around 1950 and the mid-1970s are also captured by our reconstruction.

[43] To investigate potential large-scale climate variations associated with decadal River Murray streamflow variations, we examined their links to the IPO. Power *et al.* [1999] demonstrated links between decadal-scale variations in Australian streamflow and the IPO. We confirm a similar association between 11 year smoothed IPO and naturalized River Murray streamflow observations with a correlation of -0.62 over the 1892–1988 period. The relationship between 11 year smoothed IPO and our River Murray streamflow

Table 6. Periods of Decadal-Scale High and Low Reconstructed Streamflow for the River Murray^a

River Murray High-Streamflow Periods	IPO Negative Phases	River Murray Low-Streamflow Periods	IPO Positive Phases
1820–1831	1800–1823	1788–1789	1788–1799
1856–1865	1855–1870	1794–1797	1824–1854
1874–1875	1874–1898	1810–1817	1899–1918
1883–1896	1919–1925	1834–1843	1926–1945
1911–1915	1946–1960	1852–1853	1961–1964
1947–1958 (3)	1965–1971	1867–1873	
1969–1976 (5)		1899–1909 (1)	
		1921–1928	
		1934–1944 (2)	
		1961–1964 (4)	
		1980–1982	

^a“High” and “low” are defined as periods when the decadal streamflow anomaly was at least 0.5 standard deviations from the 1892–1988 mean. Sustained negative and positive phases of Interdecadal Pacific Oscillation (IPO) variability are also described, with reconstructed IPO derived from the unified ENSO proxy [McGregor et al., 2009]. Periods in the reconstruction that are similar to those in the naturalized record are labeled from 1 to 5 and are given in parentheses. The corresponding periods in the naturalized record are period 1, 1897–1911; period 2, 1937–1946; period 3, 1950–1960; period 4, 1962–1966; and period 5, 1969–1978 (described further in section 3.2) and differ slightly from the reconstruction only in terms of onset or duration. Only the high-flow period from 1917 to 1922 in the naturalized record does not register above 0.5 standard deviations in the reconstruction.

reconstruction over the same period is stronger ($r = -0.80$) than for naturalized streamflow observations. The stronger correlation for the reconstruction compared to the observations probably reflects the fact that the remote proxy network captures more of the large-scale low-frequency variability. Conversely, the naturalized streamflow includes more high-frequency aspects of local hydroclimate variability that cannot be captured by the remote proxies.

[44] To examine the relationship of the IPO and our River Murray streamflow reconstruction prior to the 20th century, we compared the ensemble-median decadal streamflow reconstruction with a recently published IPO reconstruction [McGregor et al., 2009]. An 11 year running mean of the unified ENSO proxy (UEP) developed by McGregor et al. [2009] was chosen as an index representative of the IPO. The UEP represents the first uncalibrated EOF of 10 published ENSO reconstructions back to A.D. 1650 (see McGregor et al. [2009] for further details). As a number of the western Pacific paleoclimate records used in a previous ENSO reconstruction [Braganza et al., 2009] are used in the current study, the UEP was recalculated, removing the Braganza et al. [2009] data to provide an independent comparison. The correlation between the 11 year running mean of McGregor et al.’s [2009] IPO reconstruction and the observed IPO index [Power et al., 1999] is 0.61 over the 1897–1971 period.

[45] Figure 7 compares the decadal River Murray streamflow reconstruction with phases of the 11 year smoothed

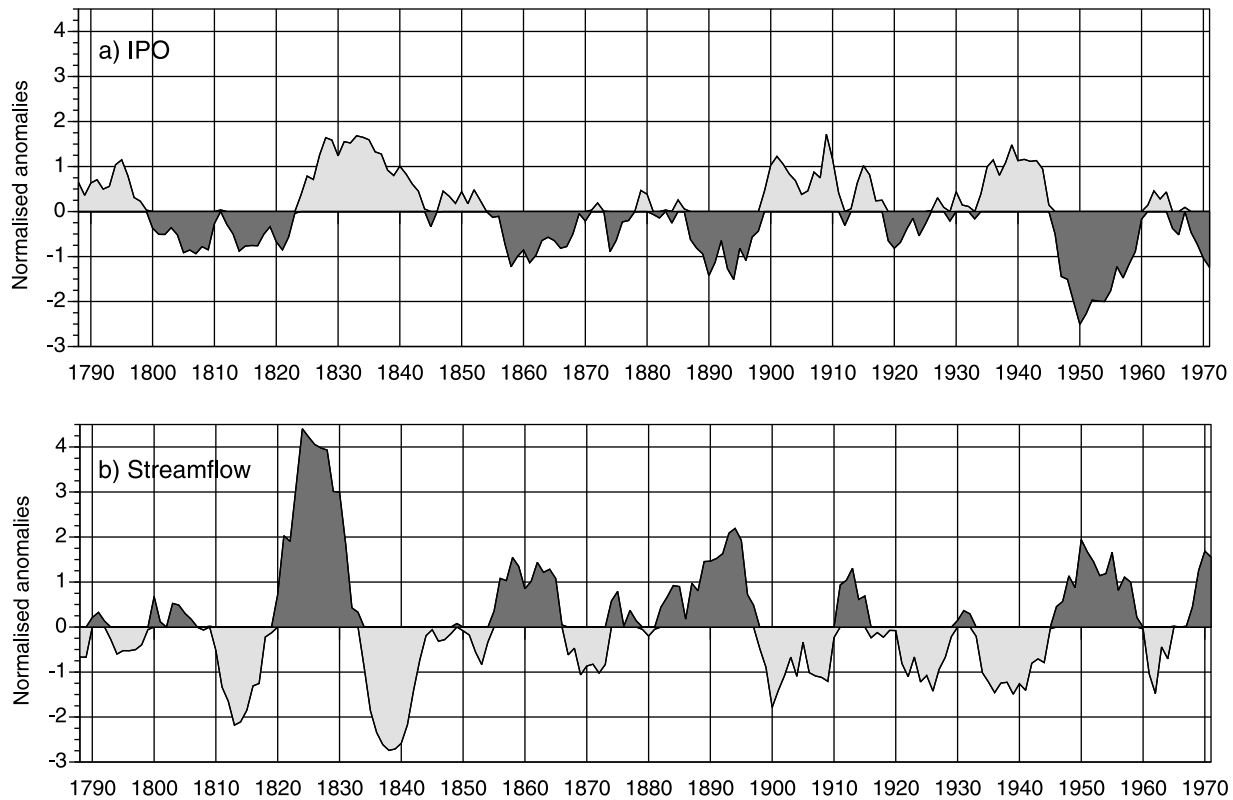


Figure 7. Reconstructed time series of the 11 year smoothed (a) unified ENSO proxy from McGregor et al. [2009], representing decadal-scale Pacific oscillations similar to the Interdecadal Pacific Oscillation and the Pacific Decadal Oscillation, and b) decadal River Murray streamflow from this study. Both time series span the period 1788–1971. Dark gray (light gray) shading corresponds to negative IPO and high-streamflow (positive IPO and low-streamflow) phases.

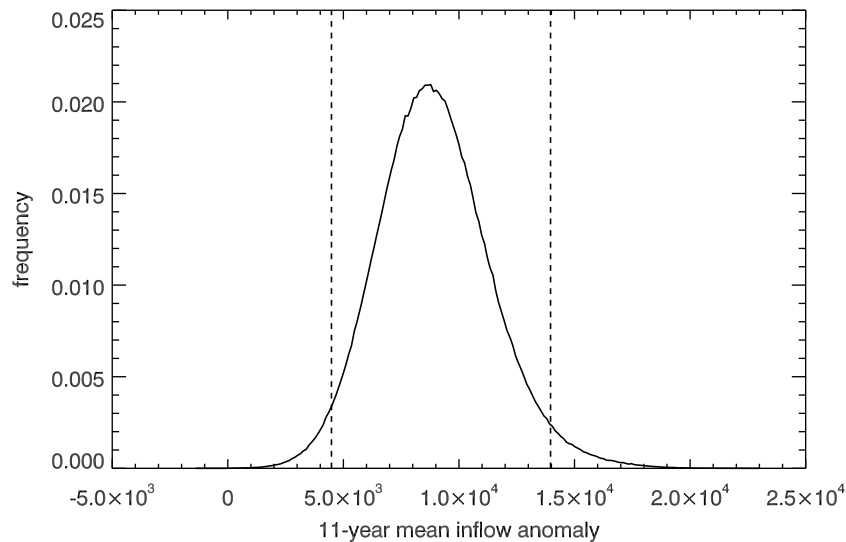


Figure 8. The distribution of all reconstructed River Murray streamflow estimates from the 10,000 member ensemble. The dashed lines represent the 1998–2008 record low naturalized streamflow of 4485 GL (left line) and the 1950–1960 record high naturalized streamflow of 13,963 GL (right line).

UEP index that represents an IPO-like signal. As seen in Table 6, the UEP shows six positive and six negative IPO phases over the 1788–1971 period, while our streamflow reconstruction shows 7 high-streamflow periods and 11 low-flow periods. The UEP and reconstructed River Murray streamflow variability tracked closely during the 20th century, which is consistent with the strong relationship identified using the instrumental IPO index. However, the relationship is more complex in the 19th century. Notably, a high-flow period beginning in 1820 corresponds to positive IPO conditions spanning the 1824–1854 period. According to the established 20th century relationships presented by *Power et al.* [1999], low-streamflow conditions are expected during positive IPO conditions. Assuming that both the streamflow and IPO reconstructions are valid, this potentially implies that the relationship between the IPO and River Murray streamflow is nonstationary.

[46] The decadal-scale variations in the UEP generally agree with variations in a composite PDO index developed from six PDO reconstructions, presented by *Verdon and Franks* [2006]. The exceptions include periods between approximately 1874–1898 and 1899–1918, which might reflect a Pacific Northwest bias in the reconstructions used in their analysis. Nonetheless, variations of Pacific decadal-scale variability seen during the early 19th century are in strong agreement, providing further evidence of a decoupling between Pacific decadal-scale variability and River Murray streamflow during the early 1800s.

3.3. Historical Context of High and Low River Murray Streamflow Extremes

[47] Record low River Murray streamflows were associated with the widespread drought experienced in southeastern Australia from August 1998 to July 2009. This period, hereafter referred to as the 1998–2008 drought, is the lowest observed in the naturalized record (1892–2008) with an annual average deficit over the decade of 4653 GL, or 50% below the 1892–2008 average. Conversely, 1950–1960

is the highest decadal streamflow anomaly in the naturalized record. During this period, the annual average surplus was 4825 GL, or 52% above the 1892–2008 average. Using our newly developed streamflow reconstruction, we are now able to expand the historical series to establish where the record River Murray low- and high-flow periods sit in the context of estimated streamflow variability over the past 2 centuries. To do this, we assess the record low and high flow periods observed in the instrumental record against the full ensemble of estimated River Murray streamflows from 1783 to 1988.

[48] Figure 8 shows the histogram of all values computed from the River Murray decadal streamflow reconstruction ensemble over the 1783–1988 period. From this, we calculated that there is a 2.3% (2.9%) chance that the 1998–2008 (1950–1960) streamflow deficit (surplus) has been exceeded during the 1783–1988 period. This makes the current record streamflow periods from 1950 to 1960 and from 1998 to 2008 unusual, but not necessarily unprecedented, in the context of our reconstruction. However, recall that the reconstruction does not simulate high streamflow values well (Figure 6). Specifically, high streamflow values were underestimated in the reconstruction, so the likelihood that the record high streamflow value of 1950–1960 has been exceeded in the paleoreconstruction has probably been underestimated.

[49] Using the expanded 206 year streamflow record, we also estimated the probability of the 1998–2008 deficit and 1950–1960 surplus by determining the average recurrence interval (ARI), or average return period, assumed under stationary climate conditions. Stochastic simulations of modeled paleostreamflow were generated using parameters derived from the paleoreconstructions. These simulations were used to estimate the ARI of the 1998–2008 streamflow deficit. The ARI was calculated using a technique that accounts for nonindependent data (e.g., a prolonged streamflow deficit) and determines a recurrence interval as the length of time between the onset of two successive drought periods (where

a drought period is defined as falling below a particular threshold) (see *Potter et al.* [2008] for further details).

[50] A natural log-transformed Gaussian ar1 process was used to model paleostreamflow. Each reconstruction of the 10,000-member ensemble of paleostreamflow reconstructions was used to determine the model parameters so that the stochastic simulations adequately represented the uncertainty in the paleostreamflow reconstructions. One hundred simulations were generated for each of the 10,000-parameter permutations.

[51] The stochastic simulations were first computed for periods the same length as the paleostreamflow reconstruction (206 years) to validate the statistical model. The simulations were generally able to capture the mean, variance, and autocorrelation observed in the paleoreconstructions. The shape of the streamflow distributions from the stochastic simulations and the reconstructions were compared using histograms generated from each data source. The majority of the ensemble of paleostreamflow distributions falls within the 90% confidence interval of those derived from the stochastic simulations. As when compared to the naturalized record, the skew of the upper tails of the paleostreamflow distributions were underestimated compared to the stochastic simulations (however, in this sense, the stochastic simulations behave more like the naturalized streamflow record). Stochastic simulations were then generated for 100,000 year intervals, and the ARI was determined for each simulation.

[52] The distribution of ARIs was heavily skewed to the right, so the median was calculated as the best estimate of the return period [*Potter et al.*, 2008]. From 1×10^6 simulations, the median ARI of the 1998–2008 streamflow deficit was 1491 years, with a 90% confidence interval of between 307 and 14,447 years. The median ARI of the streamflow surplus of 1950–1960 was 119 years, with a 90% confidence interval of between 40 and 2864 years. Thus, the 1998–2008 (1950–1960) River Murray streamflow deficit (surplus) can be interpreted as approximately a 1 in 1500 year (120 year) deficit (surplus) on the basis of extended estimates of decadal streamflow variability using an ensemble of paleoreconstructions.

4. Discussion

[53] The most striking feature of the River Murray streamflow reconstruction was the high-magnitude switch from very high to low streamflows from the 1820–1840s, associated with an apparent breakdown with decadal-scale variability in the Pacific Ocean at this time. In section 3.2, we confirmed the variations in Pacific climate variability using a composite PDO index from *Verdon and Franks* [2006]. However, unfortunately, no instrumental or naturalized River Murray streamflow data are currently available prior to 1892 to confirm this dramatic switch. Indeed, it is possible that the large early 19th century streamflow variations might be an artifact of our methodology or biases in the proxy data themselves. To help resolve this, two additional hydrological proxies were compared to our reconstruction to provide independent confirmation of this marked anomaly. A brief qualitative comparison of our streamflow with historical estimates of Lake George levels [*Russell*, 1877, 1887; *Jacobson et al.*, 1991] and the *McGowan et al.*

[2009] reconstruction of inflows into the headwater catchment of the River Murray are now discussed.

[54] A record estimating historical Lake George levels from 1817 to 1918 was available from historical sources [*Russell*, 1877, 1887; *Jacobson et al.*, 1991]. Lake George is a precipitation-sensitive basin that lies in a catchment adjacent to the northern boundary of the River Murray catchment area. The lake has no known outlet and has long been recognized as having highly variable levels [*Russell*, 1877, 1887; *Jacobson et al.*, 1991]. As such, the Lake George record is useful as an independent hydroclimate proxy to compare with our River Murray streamflow reconstruction.

[55] According to historical sources, record high Lake George levels occurred around 1821 [*Russell*, 1887]. *Russell* [1877, 1887] reported that the lake contained water from 1817 and 1828 and perhaps achieved its highest level during June 1823. For example, in 1821 the lake was described as a “magnificent sheet of water” and in 1824 was reported to be “20 miles long and 8 miles wide” [*Russell*, 1887, p. 30]. These years of maximum lake storage reported by *Russell* [1877, 1887] coincide exactly with the peak in streamflow in our reconstruction, which also reached its peak in the decade centered on 1824.

[56] Curiously, a low streamflow period in the *McGowan et al.* [2009] reconstruction is identified around 1820, which does not agree with either our reconstruction or nearby Lake George levels. This may reflect the fact that a single remote proxy was used in their reconstruction of River Murray streamflow, which may contain two separate problems. The first is that the reconstruction was derived from a single PDO reconstruction from China. Using one record from a single location is likely to contain much local climate noise on top of any large-scale climatic signal. Second, the assumption of a stationary relationship between that Chinese location (or River Murray streamflow) and the PDO may not be valid. Indeed, using an independent proxy record of decadal-scale Pacific variability, we showed that the wet period in the 1820s probably coincides with a period of neutral and positive IPO. These IPO conditions were also confirmed by a comparison with the *Verdon and Franks* [2006] composite PDO reconstruction. If we assume a stationary association between Pacific variability and River Murray streamflow, normal or low-flow conditions would be expected. Instead, our streamflow reconstruction displays record high flow conditions, which is in agreement with an independent comparison of Lake George levels. As such, our results suggest that decadal-scale variability influencing the River Murray hydroclimate during the 1820s may not be associated with decadal Pacific-wide variability.

[57] Declining Lake George levels are reported from 1832, culminating in the severe drought around 1840 [*Russell*, 1877]. In 1838–1839 *Russell* [1877, p. 31] states “there can be no doubt that in these two years of great drought the lake was dry” and that “the lake was dry enough to drive a team along the middle of it.” Such comments reflect an apparent rapid drying of the lake over a 14 year period from full in 1824 to completely dry in 1838 and confirms a similarly rapid drying at the same time in our River Murray streamflow reconstruction. Again, the *McGowan et al.* [2009] reconstruction is at odds, registering a period of high decadal-scale flow conditions around 1834.

[58] The agreement between our streamflow reconstruction and Lake George levels confirm the likelihood that the

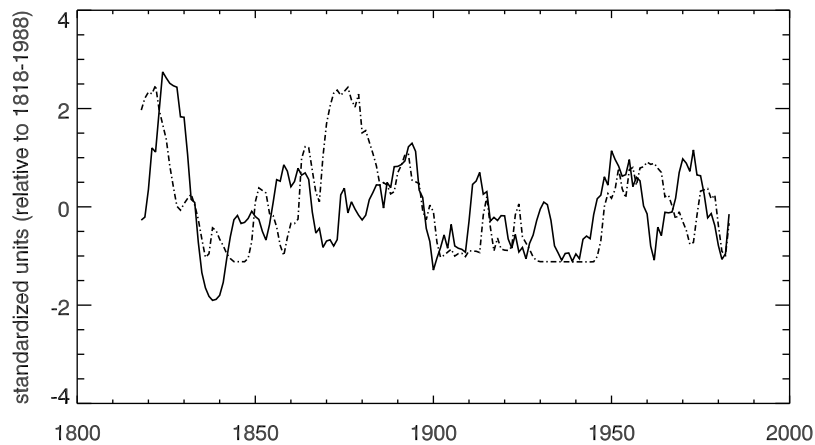


Figure 9. Time series of Lake George lake levels (dash-dotted line) and the median decadal River Murray streamflow reconstruction (solid line) from 1818 to 1988. For comparison, both time series are presented in standardized units relative to the period 1892–1988.

marked high streamflow period followed by an extreme low streamflow period in our reconstruction between 1819 and 1843 is likely to be a real feature of the regional hydroclimate variations during the early 19th century in the MDB.

[59] The Lake George record comprises data extracted from the original *Russell* [1877, 1887] records until 1904 and modern lake level measurements from various hydrological sources to 1988 [Jacobson *et al.*, 1991] (Figure 9). We caution that the early data were developed using non-standard 19th century techniques and subjective historical assessments of the lake levels from local residents. The record has not been quality controlled and therefore is likely to contain considerable uncertainties. Nevertheless, it provides us with an independent record from the MDB to make relative (rather than absolute) comparisons with our River Murray reconstruction.

[60] There is broad agreement between decadal and multidecadal scale variations in the Lake George levels and the streamflow reconstruction during most periods (Figure 9). Note that the lake levels never decrease beyond 1 standard deviation below the 1892–1988 mean, as this indicates an empty lake. The quantified record in Figure 9 contains considerable uncertainties associated with the timing and magnitudes for the reason discussed above.

[61] The wet-dry flip seen in the early 19th century is the most prominent feature of the record as is the descent into the Federation drought in the late 1890s. The broadly drier first half, and wetter second half, of the 20th century is also evident. There is divergence in the two series from the middle 1860s to the early 1880s. At this time, the Lake George data indicate wet conditions, while the streamflow reconstruction indicates normal and slightly dry conditions. Though the reason for this discrepancy is unknown, one explanation could be land surface changes associated with land clearing. From the 1860s to the 1880s much of the Lake George region experienced a substantial increase in agricultural activity with the release of Crown land to freehold ownership as part of the Robertson Selection Act of 1861 (D. Garden, personal communication, 2011). As part of the act, “improvements” to the land associated with these leaseholds included land clearance. However, the extent of the land clearance is difficult to establish (D. Garden, personal communication, 2011). Land clearance may have

increased runoff and siltation of the lake, giving the impression of high lake level rather than perhaps more plausible factors like basin aggregation and changes to land surface conditions.

5. Conclusions

[62] This study introduces a multiproxy reconstruction of River Murray streamflow from 1783 to 1988. As no paleoclimate records were available from within the River Murray catchment area, a network of nine remote proxies in regions representing climate variability from the Pacific, Southern and Indian Oceans was used to develop an experimental streamflow reconstruction. We showed that the common signal from instrumental climate data at the same locations as the paleoclimate records could be used to reconstruct a significant proportion of annual and decadal River Murray streamflow variability. After applying the same technique to the paleoclimate data network, we developed a reconstruction that was able to skillfully reproduce approximately 23% (50%) of the annual (decadal) variations in naturalized River Murray streamflow.

[63] To capture the uncertainty associated with calibrating to observations, an aspect not robustly addressed for paleoclimate reconstructions, we developed a 10,000-member ensemble of reconstructions of River Murray streamflow. The ensemble technique demonstrated that the errors associated with calibration accounted for over one quarter of the total error. From this result, we suggest that ensemble reconstruction techniques should be the focus of further work to improve the estimation of uncertainty in paleoclimate reconstructions and their subsequent interpretation.

[64] Considering all measured uncertainties in the reconstruction ensemble, we estimate that there is only a 2.3% chance that the record low 1998–2008 streamflow level in the naturalized record has been exceeded since 1783. Our reconstruction suggests that although the 1998–2008 low-flow record was not necessarily unprecedented in the 206 year record, it is still highly unusual. Further testing using synthetic simulations of streamflow based on the paleostreamflow estimates suggests that the 1998–2008 drought was a 1 in 1500 year event. Given the serious water management implications of this result, model- and process-

based studies are urgently required to determine the proportion of streamflow variations being forced by natural, decadal climate variability and anthropogenic factors.

[65] A comparison between reconstructed River Murray streamflow and low-frequency climate variability in the Pacific Ocean suggests that their relationship has not remained consistent over the past two centuries. The previously identified relationship between the two during the 20th century [Power et al., 1999] is confirmed here, adding that our study reveals that the IPO-streamflow relationship was more complex and nonstationary during the 19th century than has been observed over the instrumental period.

[66] This “proof of concept” paper demonstrates that advances in our understanding of long-term climate variability are possible through paleoclimate research. While our results are encouraging, we recognize that there is a critical need to reconstruct River Murray streamflow (and other important aspects of the Australian hydroclimate) using locally derived proxies that are far more likely to capture regional variations. That said, our successful reconstruction of streamflow variability using remote proxies indicates that even if local paleoclimate records are unavailable, important information can still be gleaned from a remote proxy network from key teleconnection regions of Australasia.

[67] We have demonstrated that high-resolution paleoclimate reconstructions offer a unique way of examining decadal, regional hydroclimate variability in the preinstrumental period, allowing us to interpret modern-day streamflow variability compared to different low-frequency mean state conditions experienced during the pre-20th century period. We recommend that future paleoclimate research efforts target variations on society-relevant time scales to increase its utility in the complex policy and natural resource management context of a rapidly warming Australia.

[68] **Acknowledgments.** A.J.E.G. is supported by an Australian Research Council (ARC) Federation Fellowship (FF0668679), and J.G. is funded by an ARC Linkage Project (LP0990151). The authors would like to thank Kathy Allen for the celery top pine tree ring chronology, Roseanne D’Arrigo for the Indonesian teak tree ring chronology, Louise Cullen and Pauline Grierson for the Western Australian *Callitris* tree ring chronology, Anthony Scott from the MDBA for providing Murray system streamflow data, Don Garden from the University of Melbourne for his advice on historical land use changes through the River Murray region, and three anonymous reviewers for their insightful comments.

References

- Allen, K. J. (2002), The temperature response in the ring widths of *Phyllocladus aspleniifolius* (celery-top pine) along an altitudinal gradient in the Warra LTER area, Tasmania, *Aust. Geogr. Stud.*, *40*, 287–299, doi:10.1111/1467-8470.00181.
- Allen, K., E. Cook, R. Francey, and K. Michael (2001), The climatic response of *Phyllocladus aspleniifolius* (Labill.) Hook. f in Tasmania, *J. Biogeogr.*, *28*, 305–316, doi:10.1046/j.1365-2699.2001.00546.x.
- Braganza, K., J. Gergis, S. Power, J. S. Risbey, and A. M. Fowler (2009), A multiproxy index of the El Niño–Southern Oscillation, A.D. 1525–1982, *J. Geophys. Res.*, *114*, D05106, doi:10.1029/2008JD010896.
- Cai, W., and T. Cowan (2008), Evidence of impacts from rising temperature on inflows to the Murray–Darling Basin, *Geophys. Res. Lett.*, *35*, L07701, doi:10.1029/2008GL033390.
- Charles, C., K. Cobb, M. Moore, and R. Fairbanks (2003), Monsoon–tropical ocean interaction in a network of coral records spanning the 20th century, *Mar. Geol.*, *201*, 207–222, doi:10.1016/S0025-3227(03)00217-2.
- Chiew, F. H. S., T. C. Piechota, J. A. Dracup, and T. A. McMahon (1998), El Niño–Southern Oscillation and Australian rainfall, streamflow and drought: Links and potential for forecasting, *J. Hydrol.*, *204*, 138–149, doi:10.1016/S0022-1694(97)00121-2.
- Cook, E., and L. Kairiukstis (1990), *Methods of Dendrochronology*, 394 pp., Kluwer Acad., Dordrecht, Netherlands.
- Cook, E., B. Buckley, R. D’Arrigo, and M. Peterson (2000), Warm-season temperatures since 1600 BC reconstructed from Tasmanian tree rings and their relationship to large-scale sea surface temperature anomalies, *Clim. Dyn.*, *16*, 79–91, doi:10.1007/s003820050006.
- Cullen, L., and P. Grierson (2009), Multi-decadal scale variability in autumn–winter rainfall in south-western Australia since 1655 AD as reconstructed from tree rings of *Callitris columellaris*, *Clim. Dyn.*, *33*, 433–444, doi:10.1007/s00382-008-0457-8.
- D’Arrigo, R., R. Wilson, J. Palmer, P. Krusic, A. Curtis, J. Sakulich, S. Bijaksana, S. Zulaikah, L. Ngkoimani, and A. Tudhope (2006), The reconstructed Indonesian warm pool sea surface temperatures from tree rings and corals: Linkages to Asian monsoon drought and El Niño–Southern Oscillation, *Paleoceanography*, *21*, PA3005, doi:10.1029/2005PA001256.
- Fowler, A., G. Boswijk, J. Gergis, and A. Lorrey (2008), ENSO history recorded in *Agathis australis* (Kauri) tree-rings Part A: Kauri’s potential as an ENSO proxy, *Int. J. Climatol.*, *28*(1), 1–20, doi:10.1002/joc.1525.
- Fritts, H. (1976), *Tree Rings and Climate*, 567 pp., Academic, New York.
- Hegerl, G. C., T. J. Crowley, W. T. Hyde, and D. J. Frame (2006), Climate sensitivity constrained by temperature reconstructions over the past seven centuries, *Nature*, *440*, 1029–1032, doi:10.1038/nature04679.
- Hegerl, G. C., T. J. Crowley, M. Allen, W. T. Hyde, H. N. Pollack, J. Smerdon, and E. Zorita (2007), Detection of human influence on a new, validated 1500-year temperature reconstruction, *J. Clim.*, *20*, 650–666, doi:10.1175/JCLI4011.1.
- Hennessy, K., B. Fitzharris, B. Bates, N. Harvey, S. Howden, L. Hughes, J. Salinger, and R. Warrick (2007), Australia and New Zealand, in *Climate Change 2007: Impacts, Adaptation and Vulnerability. Contribution of Working Group II to the Fourth Assessment Report of the Intergovernmental Panel on Climate Change*, edited by O. F. C. M. L. Parry et al., pp. 507–540, Cambridge Univ. Press, Cambridge, U. K.
- Hennessy, K. J., et al. (2008), An assessment of the impact of climate change on the nature and frequency of exceptional climatic events, *Rep. 33*, Commonw. Sci. Ind. and Res. Organ, Melbourne, Victoria, Australia.
- Jacobson, G., J. Jankowski, and R. S. Abell (1991), Groundwater and surface water interaction at Lake George, New South Wales, *J. Aust. Geol. Geophys.*, *12*, 181–190.
- Jolliffe, I. T. (2002), *Principal Component Analysis*, 2nd ed., 487 pp., Springer, New York.
- Kalnay, E., et al. (1996), The NMC/NCAR 40-year reanalysis project, *Bull. Am. Meteorol. Soc.*, *77*, 437–471, doi:10.1175/1520-0477(1996)077<0437:TNYRP>2.0.CO;2.
- Kestin, T. S. (2001), Variations of Australian climate and extremes, Ph.D. thesis, 234 pp., Monash Univ., Melbourne, Victoria, Australia.
- Kiem, A. S., and S. W. Franks (2004), Multi-decadal variability of drought risk, eastern Australia, *Hydrol. Processes*, *18*, 2039–2050, doi:10.1002/hyp.1460.
- Kiem, A. S., and D. C. Verdon-Kidd (2010), Towards understanding hydroclimatic change in Victoria, Australia—Preliminary insights into the “Big Dry”, *Hydrol. Earth Syst. Sci.*, *14*, 433–445, doi:10.5194/hess-14-433-2010.
- Kiem, A. S., S. W. Franks, and G. Kuczera (2003), Multi-decadal variability of flood risk, *Geophys. Res. Lett.*, *30*(2), 1035, doi:10.1029/2002GL015992.
- La Marche, V., J. Holmes, P. Dunwiddie, and G. Drew (1979), Tree-ring chronologies of the Southern Hemisphere: 4. Australia, Lab. of Tree Ring Res., Univ. of Ariz., Tucson.
- Linsley, B., P. Zhang, A. Kaplan, S. Howe, and G. Wellington (2008), Interdecadal–decadal climate variability from multicoral oxygen isotope records in the South Pacific Convergence Zone region since 1650 A.D., *Paleoceanography*, *23*, PA2219, doi:10.1029/2007PA001539.
- Lough, J. (2007), Tropical river flow and rainfall reconstructions from coral luminescence: Great Barrier Reef, Australia, *Paleoceanography*, *22*, PA2218, doi:10.1029/2006PA001377.
- McGowan, H. A., S. K. Marx, J. Denholm, J. Soderholm, and B. S. Kamber (2009), Reconstructing annual inflows to the headwater catchments of the Murray River, Australia, using the Pacific Decadal Oscillation, *Geophys. Res. Lett.*, *36*, L06707, doi:10.1029/2008GL037049.
- McGregor, S., A. Timmermann, and O. Timm (2009), A unified proxy for ENSO and PDO variability since 1650, *Clim. Past*, *5*, 2177–2222, doi:10.5194/cpd-5-2177-2009.

- Murphy, B. F., and B. Timbal (2008), A review of recent climate variability and climate change in southeastern Australia, *Int. J. Climatol.*, *28*, 859–879, doi:10.1002/joc.1627.
- North, G. R., T. L. Bell, R. F. Cahalan, and F. J. Moeng (1982), Sampling errors in the estimation of empirical orthogonal functions, *Mon. Weather Rev.*, *110*, 699–706, doi:10.1175/1520-0493(1982)110<0699:SEITEO>2.0.CO;2.
- Peterson, T. C., and R. S. Vose (1997), An overview of the Global Historical Climatology Network Temperature Database, *Bull. Am. Meteorol. Soc.*, *78*, 2837–2849, doi:10.1175/1520-0477(1997)078<2837:AOOTGH>2.0.CO;2.
- Potter, N. J., F. H. S. Chiew, A. J. Frost, R. Srikanthan, T. A. McMahon, M. C. Peel, and J. M. Austin (2008), Characterisation of the recent rainfall and runoff in the Murray-Darling Basin, 40 pp., Commonw. Sci. Ind. and Res. Organ, Melbourne, Victoria, Australia.
- Power, S., T. Casey, C. K. Folland, A. Colman, and V. Mehta (1999), Interdecadal modulation of the impact of ENSO on Australia, *Clim. Dyn.*, *15*, 319–324, doi:10.1007/s003820050284.
- Rayner, N. A., D. E. Parker, E. B. Horton, C. K. Folland, L. V. Alexander, D. P. Rowell, E. C. Kent, and A. Kaplan (2003), Global analyses of sea surface temperature, sea ice, and night marine air temperature since the late nineteenth century, *J. Geophys. Res.*, *108*(D14), 4407, doi:10.1029/2002JD002670.
- Risbey, J. S., M. J. Pook, P. C. McIntosh, M. C. Wheeler, and H. H. Hendon (2009), On the remote drivers of rainfall variability in Australia, *Mon. Weather Rev.*, *137*, 3233–3253, doi:10.1175/2009MWR2861.1.
- Russell, H. C. (1877), *Climate of New South Wales: Descriptive, Historical, and Tabular*, Charles Potter, Sydney, N. S. W., Australia.
- Russell, H. C. (1887), *Notes Upon Floods in Lake George*, Charles Potter, Sydney, N. S. W., Australia.
- Seager, R. (2007), The turn of the century North American drought: Global context, dynamics, and past analogs, *J. Clim.*, *20*, 5527–5552, doi:10.1175/2007JCLI1529.1.
- Shen, C., W. C. Wang, W. Gong, and Z. Hao (2006), A Pacific Decadal Oscillation record since 1470 AD reconstructed from proxy data of summer rainfall over eastern China, *Geophys. Res. Lett.*, *33*, L03702, doi:10.1029/2005GL024804.
- Verdon, D. C., and S. W. Franks (2006), Long-term behaviour of ENSO: Interactions with the PDO over the past 400 years inferred from palaeoclimate records, *Geophys. Res. Lett.*, *33*, L06712, doi:10.1029/2005GL025052.
- Verdon, D. C., and S. Franks (2007), Long-term drought risk assessment in the Lachlan River Valley—A paleoclimate perspective, *Aust. J. Water Resour.*, *11*, 145–152.
- Verdon-Kidd, D. C., and A. S. Kiem (2009), Nature and causes of protracted droughts in southeast Australia: Comparison between the Federation, WWII, and Big Dry droughts, *Geophys. Res. Lett.*, *36*, L22707, doi:10.1029/2009GL041067.

A. J. E. Gallant and J. Gergis, School of Earth Sciences, University of Melbourne, Melbourne, Vic 3010, Australia. (agallant@unimelb.edu.au)